HHS Public Access

Author manuscript

Neuroimage. Author manuscript; available in PMC 2021 October 07.

Published in final edited form as:

Neuroimage. 2020 April 01; 209: 116515. doi:10.1016/j.neuroimage.2020.116515.

The disengaging brain: Dynamic transitions from cognitive engagement and alcoholism risk

Enrico Amico[1,2], **Mario Dzemidzic**[3], **Brandon G. Oberlin**[3,4], **Claire R. Carron**[3], **Jaroslaw Harezlak**[5], **Joaquín Goñi**[1,2,6,*,†], **David A. Kareken**[3,*,†]

[1.] Purdue Institute for Integrative Neuroscience, Purdue University

[2.] School of Industrial Engineering, Purdue University

[3.] Department of Neurology, Indiana University School of Medicine; Indiana Alcohol Research Center

[4.] Department of Psychiatry, Indiana University School of Medicine

[5.] Department of Epidemiology and Biostatistics, Indiana University

[6.] Weldon School of Biomedical Engineering, Purdue University

Abstract

Human functional brain connectivity is usually measured either at “rest” or during cognitive tasks, ignoring life’s moments of mental transition. We propose a different approach to understanding brain network transitions. We applied a novel independent component analysis of functional connectivity during motor inhibition (stop signal task) and during the continuous transition to an immediately ensuing rest. A functional network reconfiguration process emerged that: (i) was most prominent in those *without* familial alcoholism risk, (ii) encompassed brain areas engaged by the task, yet (iii) emerged only transiently after task cessation. The pattern was not present in a pre-task rest scan or in the remaining minutes of post-task rest. Finally, this transient network reconfiguration related to a key behavioral trait of addiction risk: reward delay discounting. These novel findings illustrate how dynamic brain functional reconfiguration during normally unstudied periods of cognitive transition might reflect addiction vulnerability, and potentially other forms of brain dysfunction.

[*]Corresponding authors: jgonicor@purdue.edu, dkareken@iu.edu.
[†]Both authors equally contributed

Author Contributions

D.K. and M.D. conceptualized and designed the fMRI study; C.C. and M.D. collected and acquired the dataset; E.A., M.D. and J.G. processed the MRI data; E.A. and J.G. designed the framework and performed the connectivity analyses; M.D. performed the stop signal task analysis; B.G.O. programmed the delay discounting task and performed analyses; all authors interpreted the results; E.A., M.D., J.G., B.G.O., and D.K wrote the manuscript.

Competing Financial Interests

The authors declare no competing financial interests.

Code availability

The connICA code (in MATLAB) used for this analysis is freely available at the CONNplexity Lab website: https://engineering.purdue.edu/ConnplexityLab/publications

Introduction

Functional organization of the human brain is usually assessed either at “rest” (quiet introspection without external task demands) or during tasks requiring goal-directed behavior (Gonzalez-Castillo and Bandettini 2018). Yet a rigid distinction between rest and directed mental effort fails to capture the critical periods of mental state transitions that characterize the cognitive demands of daily life. Rather, everyday life demands frequent transitions between introspection, when the brain’s default mode network (DMN) activity is prominent (Raichle et al. 2001; Shulman et al. 1997), and goal-directed behaviors supported by “task positive” networks (Cole et al. 2014; Shine et al. 2017).

At odds with a simplistic rest-task dichotomy is the presence of task-like connectivity within periods of rest (Chen et al. 2018). “Resting” connectivity is also different in the immediate wake of mental effort when compared to rest after a longer period of time (Amico et al. 2019; Chen et al. 2018; Lewis et al. 2009; Pyka et al. 2009). As opposed to a simple binary switch from active to resting brain, a sequence of network functional reconfigurations is likely needed *en route* to rest (Shine et al. 2017). Moreover, the nature of dynamic brain reconfiguration appears central to higher-order thinking, as better cognitive performance is associated with small, efficient updates in brain connectivity across states of rest and task engagement (Schultz and Cole 2016). By extension, such dynamic network reconfigurations would also seem a plausible marker of psychiatric disease liability. This creates a need for new ways of examining brain network functional reconfiguration in humans.

Here we investigated how brain state transitions and their associated functional connectomes relate to a family history of alcoholism (FHA). FHA is not only one of the strongest predictors of developing an alcohol use disorder, but it is also a risk factor for other behavioral disorders (Heiman et al. 2008; Moss et al. 2007; Nurnberger et al. 2004b; Walters et al. 2018). Executive brain areas seem a prime target of study, as evidence indicates that executive control of behavior is both heritable and impaired in the offspring of alcoholic parents (Dougherty et al. 2015; Gustavson et al. 2017; Nigg et al. 2004; Young et al. 2009). Similarly, the frontal brain anatomy and function that undergird executive behaviors have been shown to be affected by FHA and predict binge drinking (Cservenka 2016; Hardee et al. 2014; Porjesz et al. 2005; Whelan et al. 2014).

An important aspect of executive function involves efficient changes in connectivity between mental states (Braun et al. 2015; Gallen et al. 2016; Schultz and Cole 2016; Shine et al. 2019). Furthermore, (Acheson et al. 2014) showed that, in a Go/No-Go motor inhibition paradigm, those with FHA had greater blood oxygenation level dependent (BOLD) activity during both blocks of mixed Go and No-Go (inhibitory) stimuli, as well as blocks of Go stimuli alone (each block compared to baseline). As commented upon by (Colrain 2015), several of these regions of greater BOLD activity in the FHA group comprised nodes in the default mode network (DMN). Although the Acheson, et al. study involved directed cognitive effort, the DMN is a network that is most prominent at “rest” (Raichle et al. 2001; Shulman et al. 1997). While other explanations for the Acheson et al. findings are possible, they could arise if those with FHA deactivate less between trials (i.e., during brief periods

of lower response demands). In the context of data indicating that task-induced BOLD activation magnitude relates to resting connectivity strength (Mennes et al. 2010), these collective observations led us to hypothesize that FHA might involve altered connectivity patterns or reconfiguration processes when transitioning between mental states of high and low cognitive demand.

We therefore designed a study in which we could test for FHA-related connectivity differences during the transition from active behavioral engagement (motor inhibition in the stop signal task; SST) to rest. We tested our hypothesis using a novel data-driven, connectivity-based independent component analysis (connICA (Amico et al. 2017)). The results of this analysis revealed a specific functional reconfiguration process that: (i) was associated with FHA, (ii) encompassed a number of brain areas actively engaged by the task, yet (iii) emerged during the subsequent rest period, (iv) and only transiently during an approximate 3 minute period, 15–20 seconds after task cessation. Critically, (v) the reconfiguration was *not* present in a pre-task rest scan, or in the final four minutes of rest. Finally, a *post-hoc* analysis in a subset of subjects revealed associations between the prominence of this functional reconfiguration process and a key addiction-related trait behavioral risk: delay discounting of reward.

These novel findings provide a critical foundation for understanding how brain functional networks reconfigure in task transitions, and how this dynamic reorganization relates to potential markers of brain dysfunction.

Methods

Subject information.

All subjects signed an informed consent prior to study procedures, all of which were approved by the Indiana University Institutional Review Board. Fifty four subjects (23 positive FHA, mean age= 23.0, SD= 1.6, 9 men; 31 negative FHA, mean age= 22.4, SD= 1.6, 16 men; Table 1) completed fMRI. Subjects were classified as FHA positive if they had at least one first degree relative with a history of alcoholism. Subjects were classified as FHA negative if they had no first or second degree relatives with any history of alcoholism. Family history was established by interviewing the subject using the family history module of the semi-structured assessment for the genetics of alcoholism (SSAGA; (Bucholz et al. 1994)). Three FHA positive subjects had affected mothers, but reported that their mothers did not drink during pregnancy. These three subjects had between two and four years of college education, had no obvious facial abnormalities as reported by the interviewing technicians, and had go and stop signal reaction times (see below) within one standard deviation of the remainder of the sample.

Stop Signal Task.

The SST was programmed using E-Prime 2.0 software (Psychology Software Tools Inc., Sharpsburg, PA), and consisted of 54 Go trials and 26 Stop trials. Go trials required a left or right button press on an MRI-compatible button box (Current Designs, Philadelphia, PA) to horizontal blue arrows pointing left or right. Subjects were instructed to respond as quickly

and as accurately as possible. Stop trials occurred immediately after a Go stimulus, and were signaled by a red up-pointing arrow, indicating the need to inhibit the Go response. An adaptive staircase algorithm adjusted the delay between Go and Stop stimuli in 50 ms increments to target a stop inhibition rate of 50%. Estimated stop signal response time (SSRT) was calculated by subtracting a subject's average stop-signal delay from that subject's x^{th} percentile Go RT, where x corresponds to the stop failure rate (Band et al. 2003). Thus, if a subject failed to stop on 45% of stop trials, the Go RT subtracted from the average stop-signal delay would be that of the 45^{th} percentile of the subject's Go RT distribution. A mirror on the head coil permitted subjects to view stimuli as back-projected on a screen at the rear of the scanner bore. Prior to imaging, subjects briefly practiced the task (8 Go and 7 Stop trials) on a laptop outside the imaging suite.

Delay Discounting Task.

Prior to MRI, subjects also performed a delay discounting task on a laptop outside the scanner. The task was programmed using E-Prime 2.0 software (Psychology Software Tools Inc., Sharpsburg, PA), and consisted of 60 binary choice trials; 5 trials for each of the 6 delays, duplicated for $20 and $200 standard amounts. An adaptive staircase procedure adjusted the immediate amount (initially half the standard) down for immediate choices and up for delayed choices, converging on the subjective preference for immediate money across delays (Du et al. 2002). Delays were 2 days, 1 week, 1 month, 6 months, 1 year, and 5 years. Amount/delay combinations and the presentation side were pseudorandomized. The task was not implemented in the first four study subjects, while data for four additional subjects were excluded for nonsystematic discounting of >25% deviation (based on (Johnson and Bickel 2008)), resulting in a sample of n=46. There were no significant group differences in the demographics reported in Table 1 between the n =8 subjects left out and the n=46 sample with available delay discounting data.

MRI Acquisition.

Subjects were imaged on a 3T Siemens Prisma MRI scanner with a 64-channel head coil, and with neck elements turned off. For both (rest and task-rest) functional MRI scans, we employed a multi-band (MB) blood oxygenation level dependent (BOLD) contrast sensitive sequence as detailed in Xu et al. (Xu et al. 2013): gradient-echo echo-planar imaging (GE-EPI), MB slice acceleration factor 3, repetition/echo time TR/TE=1,200ms/29ms, flip angle 65˚, 2.5×2.5×2.5 mm^3 voxels, 220mm x 220mm field of view, 54 interleaved axial slices. Two BOLD fMRI scans were performed: 1) 8:07 min (400 volumes) scan at rest while subjects fixated on a central white cross-hair and 2) 12:19 min scan (610 volumes) scan consisting of 4 minutes of the SST performance, followed by a short 12 sec transition period when a slide announced an upcoming 8 min rest. BOLD volumes during first 7 sec of each scan were not considered to allow for calibrations and MR signal reaching steady state magnetization. Therefore, BOLD data assessed consisted of two fMRI scans of 8:00 and 12:12 min respectively (Fig 1A for overview of the sequence of acquisitions).

Two short (16 sec) spin echo EPI scans (TR/TE=1560/49.8ms, five in A-P and five in P-A phase direction) with an imaging volume and voxel size identical to the GE-EPI were acquired immediately before each BOLD fMRI scan. These phase-reversed spin

echo EPI scans provided field map for correcting EPI geometric distortion (Smith et al. 2004). This procedure was performed using FSL's topup/applytopup (Smith et al. 2004), which yielded improved signal localization across the whole brain, with the most notable improvements in frontal and temporal areas (Smith et al. 2004). At the start of the imaging session and preceding the spin echo EPI scans, subjects received a T1-weighted anatomical MRI with whole brain coverage using a 3D Magnetization Prepared Rapid Gradient Echo (MPRAGE) sequence (5:12 min long, 176 sagittal slices, $1.1\times1.1\times1.2mm^3$ voxels, GRAPPA R=2 acceleration) per the Alzheimer's Disease Neuroimaging Initiative (ADNI-2) imaging protocol.

Preprocessing.

fMRI data were processed with an in-house developed pipeline based on Matlab and FSL using state-of-the-art guidelines (Amico et al. 2017; Power et al. 2012; Power et al. 2014). These steps included: BOLD volume unwarping with *applytopup*, slice timing correction (*slicetimer*), realignment (*mcflirt*), normalization to mode 1000, demeaning and linear detrending (Matlab *detrend*), regression (Matlab *regress)* of 18 signals: 3 translations, 3 rotations, and 3 tissue-based regressors (mean signal of whole-brain, white matter (WM) and cerebrospinal fluid (CSF)), as well as 9 corresponding derivatives (backwards difference; Matlab). A scrubbing procedure censoring high head motion volumes was based on two metrics: Frame Displacement (FD, in mm), and DVARS (D referring to temporal derivative of BOLD time courses, VARS referring to root mean square variance over voxels) from Power et al. (Power et al. 2014). Specifically, we used the standardized DVARS as proposed in Afyouni et al. (Afyouni and Nichols 2018). We also used SD (standard deviation of the BOLD signal within brain voxels at every time-point). The FD and DVARS vectors (obtained with *fsl_motion_outliers*) were used to tag outlier BOLD volumes with FD > 0.3 mm and standardized DVARS > 1.7. The SD vector obtained with Matlab was used to tag outlier BOLD volumes higher than 75 percentile + 1.5 of the interquartile range per FSL recommendation (Jenkinson et al. 2012). Note that there was no significant difference in the number of censored volumes between the two FHA groups (p= 0.15 for the first resting-only fMRI scan, p= 0.35 for the second, task-rest scan, two-tailed t-test).

A bandpass first-order Butterworth filter [0.009 Hz, 0.08 Hz] was applied to all BOLD time-series at the voxel level (Matlab *butter* and *filtfilt*). The first three principal components of the BOLD signal in the WM and CSF tissue were regressed out of the gray matter (GM) signal (Matlab, *pca* and *regress*) at the voxel level. A whole-brain data-driven functional parcellation based on 278 regions, as obtained by Shen et al. (Shen et al. 2013), was projected into each subject's T1 space (FSL *flirt* 6dof, FSL *flirt* 12dof and finally FSL *fnirt*) and then into native EPI space of each subject. We also applied FSL boundary-based-registration (Greve and Fischl 2009) to improve the registration of the structural masks and the parcellation to the functional volumes. For the subcortical nodes, we implemented striatal regions as defined by Mawlawi et al. (Mawlawi et al. 2001) and thalamic regions defined by Behrens et al. (Behrens et al. 2003). The thalamic regions were further consolidated from 7 to 4 per hemisphere (pre-motor, primary motor, and sensory input regions were combined, and occipital and temporal-projecting regions were combined). This procedure resulted in a total number of 286 brain regions.

We estimated individual functional connectivity matrices using Pearson's correlation coefficient between the averaged signals of all region pairs. The resulting individual FC matrices were comprised of 286 cortical and subcortical nodes. Finally, the resulting functional connectomes were ordered according to seven cortical resting state networks (RSNs) as proposed by Yeo et al. (Yeo et al. 2011)(see insert of Fig. 2B). For completeness, we added two more networks: one comprised of the subcortical and one of the cerebellar regions.

Connectivity independent component analysis (connICA) on Family history of alcoholism (FHA) data.

connICA is a novel data-driven methodology that applies independent component analysis (Amico et al. 2017) to extract independent connectivity patterns from individual functional connectomes. connICA's output includes: i) an "FC-component" representing an independent pattern of functional connectivity present across subjects, and ii) each subject's weight, quantifying the (signed) component strength or prominence in each individual FC matrix (see Fig. S1). connICA has been recently used in disentangling connectivity subsystems associated with levels of consciousness (Amico et al. 2017), Alzheimer's disease (Contreras et al. 2017), as well as in extracting "hybrid" connectivity features from sets of functional and structural connectomes (Amico and Goñi 2018).

Static functional connectivity analyses.—We divided both scans into 4-min periods (Fig. 1A), two during the baseline rest scan and three during the task-rest scans (TASK - first 4 minutes [omitting a 12 sec slide instruction], REST POST1 - subsequent 4 minutes, and REST POST2 window - last 4 minutes). We then applied connICA separately in each 4-min block, testing for independent functional components or "components of interest" that significantly differentiated FHA (Fig. 1B). A component of interest must be (i) robust (appear in multiple ICA runs) and (ii) as per our hypothesis, associated with FHA during the task-rest fMRI scan (which includes SST, REST POST1 and REST POST 2 blocks; see Figure 1). Given the non-deterministic nature of the ICA decomposition into components (Hyvarinen 1999; Hyvärinen and Oja 2000), multiple ICA runs are required to select the most robust outcomes (Amico et al. 2017; Hyvarinen 1999). As in previous work, we accounted for this by evaluating the robustness of the components ("FC-traits" in (Amico et al. 2017)) over 100 FastICA runs. The FC-component was considered robust when it appeared in at least 75% of the runs, as defined by a correlation of 0.75 or higher across runs (Amico et al. 2017).

Before running the connICA algorithm, we applied Principal Component Analysis (PCA (Jolliffe 2014)) to perform noise filtering and dimensionality reduction, as recommended by work in machine learning (Särelä and Vigário 2003) and neuroimaging communities (Calhoun et al. 2006; Kessler et al. 2014). After this PCA-based preprocessing, we estimated the number of independent components (Amico et al. 2017; Calhoun et al. 2009). The two parameters of percent retained variance from PCA and number of independent components were broadly explored to find the optimal combination. For each block, we examined percent variance retained after PCA in the range [75%, 100%], in steps of 5%. Similarly, we evaluated the number of ICA components in the range [5, 25], in steps of 5. An optimal

choice was defined as *numRobustcomps (%) × numICAconvergence (%)*, i.e. where the number of robust components and the convergence of the fastICA algorithm across runs were both maximized (see supplementary Fig. S2). As depicted in Fig. S2, the optimal choice of these two parameters was 85% retained variance in PCA and 15 independent components. Importantly, family history of alcohol or any other subject characteristic *was not* considered during this evaluation.

Anatomic similarities between a component of interest and an activation map for the [Stop>Go] BOLD contrast during the stop signal task.—We evaluated the spatial overlap between a component of interest obtained through connICA and brain regions engaged by the stop signal task as follows: 1) The FC component of interest was summarized by the (positive) strength of brain regions by summing their positive connectivity values, which were assigned a corresponding percentile rank based on their distribution. 2) We then created voxel-level nodal strength masks in one-percentile increments from the 50th to the 90th percentiles. 3) We assessed the overlap between the nodal strength mask and the activation map ([Stop > Go] contrast, $p<0.05$ family-wise error (FWE), cluster-corrected using a $p=0.001$ cluster forming threshold). 4) We computed the (i) percentage of voxels and (ii) the number of voxels within both the nodal strength mask and the activation mask. 5) We then developed a null model to assess overlap between the two masks that would be expected from chance distributions of the gray matter voxels. Specifically, for each percentile threshold assessed on the nodal strength map, the null distribution was created by randomly shuffling the voxels of the nodal strength mask in the gray matter 1,000 times, while keeping the [Stop > Go] activation mask fixed.

Dynamic functional connectivity analyses.—To refine the estimate of when any components of interest emerged, we employed a standard rectangular sliding window approach with four different window lengths (60, 75, 90 and 120 seconds, sliding in 6 second increments) and extracted dynamic functional connectomes (dFC) in each window. For every window we ran connICA using fixed parameters from the static case, specifically: 100 runs, 75% criteria for robust independent components, 85% PCA variance retained, 15 ICA components (see previous section for details). This same procedure was repeated 25 times in a *leave-two-out* fashion (one subject per group, one FHA negative and one FHA positive), to diminish the influence of possible outliers. For each identified component of interest, we proceeded as follows. For each sliding window (and for each leave-two-out run), the component of interest was correlated with the dynamic robust functional components found during both fMRI scans (i.e., both baseline rest and task-rest scans). The inclusion of both scans was needed to show that the component of interest was specific to the task-rest scan (i.e., not present during the baseline rest). To capture the dynamics of a component of interest along the course of the two fMRI scans, the best-matching dFC component (i.e. the one with the highest correlation in absolute value with the static component of interest) was reported within the sliding time window. Similarity between components was measured by a Pearson's correlation coefficient between the (vectorized) full connectivity profiles.

Results

FC Component Derivation.

We employed an innovative data-driven independent component analysis of functional connectomes (connICA (Amico et al. 2017), also see Fig. S1) on fifty four subjects (23 with at least one first degree relative with alcoholism, 31 with no first or second degree relatives with alcoholism; see Table 1). In the “static” connICA step, we evaluated each of the five fMRI blocks (i.e. REST PRE1, REST PRE2, SST, REST POST1, REST POST2, each 4-minute long, see Fig. 1B and Methods for details). The aim was to search for a functional connectivity (FC) signature associated with family history of alcoholism (FHA) that we hypothesized would manifest solely during the post-task resting block. The procedure can be summarized as follows (see Methods section for details): 1) We first determined the optimal number of robust independent components, which turned out to be 15 for this dataset (see Fig. S2 caption for details). 2) Only those components that satisfied the robustness criterion were tested for associations with FHA. 3) The sole component found to be associated with FHA was then used in a sliding-window analysis to better characterize when it emerged and disappeared.

During the task-rest scan, connICA extracted 30 robust components: 12 during the SST, 11 during REST POST1 (see Fig. S4) and 7 during REST POST2. Among those, the static connICA data-driven analysis (Fig. 1B) resulted in a single component in REST POST1 that distinguished the FHA groups, as evident in group differences of the component weights. These weights were significantly lower in the FHA positive subjects (two-tailed t-test, uncorrected $p=0.0023$; false discovery rate (FDR, (Benjamini and Hochberg 1995)) adjusted $p=0.04$, accounting for the 30 robust components; Fig. 2A3), indicating that they had a diminished presence of this component.

The component emerged only during the 4 minute rest following the task (i.e., REST POST1 block, Fig. 1) and was absent in the SST block and other three resting state blocks (i.e. REST PRE1, REST PRE2 and REST POST2). This FHA-Differentiating Component (FHA-DC) predominantly encompassed functional connectivity between the visual and dorsal attentional areas, and between associative visual areas and default-mode/fronto-parietal networks (Fig. 2A1-A2, Fig. 2B1-B2). Specifically, FHA-DC showed associative visual areas positively coupled with dorsal attentional cortices, as well as negatively coupled with default-mode/fronto-parietal networks (Fig. 2A1-A2, Fig. 2B1-B2). We repeated this analysis after excluding the three FHA positive subjects whose first degree relatives were mothers with alcoholism (i.e., despite subject reports to the contrary, to rule out any possible effect of significant fetal alcohol exposure). The FHA-DC remained present in the REST POST1 block (FHA-DC similarity with full (n=54) sample of $r= 0.9$).

To assure that the FHA-DC component found through connICA was not dependent on the selected number of independent components (estimated to be 15 in this manuscript, see also Fig. S2), we tested for the presence of the FHA-DC across different numbers of derived components (from 11 to 20 in steps of 1; 100 realizations for each number of components evaluated). The component was identified ($r >0.95$) for more than 80% of the realizations (see Fig. S3 for details).

FC Component Predictors.

To better understand this functional reconfiguration component, we performed a multi-linear regression analysis to predict FHA-DC weights based on four FHA-related predictors. Specifically, FHA group membership, and three variables on which FHA groups differed: CESD scores measuring depressive symptoms, AUDIT scores reflecting alcohol use disorder symptoms, and recent self-reported drinking as assessed by grams of alcohol per week normalized by total body water to account for sex differences (Fig. 3A-B-C, also see Table 1). Four nuisance variables were also included to account for any potential effects of age, sex, head motion (number of scrubbed volumes, see Methods for details), and stop signal response time (SSRT, in milliseconds) to control for individual differences in motor inhibition during SST. In the multilinear model, sex was a significant effect (p=0.02, Fig. 3A), while depression scores (CESD) showed trend-level significance (p=0.058, Fig 3A). Notably, after accounting for these factors, the between group difference in the FHA-DC was also a significant predictor of the multi-linear regression model (p=0.0011, Fig. 3A). The linear relationship between the actual and predicted weights explains about 45% of the variance in the FHA-DC individual weights (Fig. 3B), with well-behaved residuals. Specifically, the residuals are symmetrically distributed, tending to cluster around 0, and within 2.5 standard deviations of zero (Fig. 3C).

Anatomic Similarities Between the FC component and Stop Signal Task Functional Anatomy.

To assess spatial overlap between brain regions active during SST (e.g., responses to Go and correct Stop trials; see Fig 1A and Methods) and the FHA-DC subsystem observed during the transition to rest, we used trial-specific responses during SST (voxel-wise t-statistic maps, FWE cluster-corrected at p<0.05, p=0.001 cluster-forming threshold) and the top 25% most prominent brain “hubs” (in terms of positive nodal strength, Fig. 2B1) in FHA-DC. Specifically, the anatomic hubs of FHA-DC cover, on average, 18% ±1% standard error (SE) of the Go trials’ activation (Fig. 4B1, yellow bars); the Stop trials’ activation coverage is 29% ±1% SE (Fig. 4B2, yellow bars). Notably, the overlap is most extensive for the Stop compared to Go trials contrast (Fig. 4A3, also see (Kareken et al. 2013)). Particularly, the [Stop > Go] activation map coverage is 43% ±2% SE (Fig. 4B3, yellow bars). Furthermore, additional analyses spanning a wide range of nodal hub strengths (50^{th} to 90^{th} percentile rank) showed that the overlap between the FHA-DC and the [Stop > Go] activation map exceeded chance as defined by a spatial null model (see Figure S5 and Methods for details on the null model).

Most importantly, the stop signal activation maps in each subject are computed in SPM12 during the SST block and derived using *a priori* general linear model-based analyses of the blood oxygenation level dependent (BOLD) response modeled with a standard hemodynamic response function, completely independently of the connectivity analyses. Furthermore, the FH group effects assessed with independent two-sample t-tests in SPM12 showed no differences (peak voxel p<0.05, family wise error (FWE)-corrected for multiple comparisons across the whole brain at a cluster-forming threshold of p=0.001) in BOLD activation for each of the reported SST contrasts (Go, Stop, and Stop > Go). Also note that the applied thresholds for both SST activation and nodal strength connectivity maps

emphasize the most prominent brain regions in both analyses, which lends an additional credence to the observed overlap between task activation and the anatomic distribution of the FHA-DC.

Dynamic connICA analysis.

Of particular interest was the fact that, although the major hubs in the FHA-DC encompass brain circuitry that was strongly elicited by the SST, this component emerged only in the subsequent 4 minutes of rest (i.e., REST POST1). That is, the FHA-DC *did not manifest during the task,* but well after the task-induced hemodynamic response has decayed. To narrow the temporal dynamics of the FHA-DC in REST POST1, and determine if it was specific for that time period, we ran a post-hoc connICA analysis with a finer temporal resolution (2 min sliding window rather than "static" non-overlapping 4 min intervals) across both fMRI scans. Consistent with the static results, the FHA-DC was absent during the baseline rest (Fig 5A), began only after task completion, and lasted transiently for approximately 3 minutes (Fig. 5B). These findings suggest that the connectivity component sensitive to differences in FHA occurred as subjects switched from the task itself *en route* to a state of quiet rest. We also explored shorter sliding windows and found the FHA-DC peak to be present, albeit less prominently, for 90 and 75 sec window durations before fading at the 60 sec window duration (Fig. S6). The temporal (i.e., onset and duration) and spatial (i.e., overlap with regions in a preceding task) characteristics of this component suggest its involvement in functional reconfiguration of the brain networks in the transition from cognitive effort to rest.

Relationship to impulsivity.

Finally, we explored the extent to which behavioral impulsivity— a key feature of addiction risk (Amlung et al. 2017; Bickel et al. 2007)— related to the FHA-DC. Specifically, a subset of subjects ($n = 46$) had data available from a delay discounting paradigm, which quantifies subjects' devaluation of money as a function of delay to receipt. This "reward impatience" is a phenotype common to various addictions (Amlung et al. 2017; Bickel et al. 2007) and longitudinally predicts drug use (Fernie et al. 2013) and treatment outcomes (MacKillop and Kahler 2009; Stanger et al. 2012). The area under the delay discounting curve (AUC) was significantly correlated with the FHA-DC weights ($r = 0.35$, $p = 0.018$; Fig. S8C), such that greater delayed reward preference ("patience") correlated with more of the FHA-DC trait. When entered into the additive multi-linear regression model, the FHA-DC remained significant; the AUC from the delay discounting curve remained significant, as well ($p = 0.034$; Fig. S8D).

Discussion

Alcoholism is highly prevalent (Grant et al. 2015) and few affected receive treatment (Cohen et al. 2007); after treatment, drinking relapse remains clinically significant (Anton et al. 2006; Schneekloth et al. 2012). Understanding brain-related vulnerabilities is thus important to prevention and public health, especially given alcoholism's comorbidity and joint risk with other mental illness (Walters et al. 2018).

Prior research of how FHA affects brain connectivity is not extensive, with past work using *a priori* seed regions (Cservenka et al. 2014) or seed-based analyses of data collected during cognitive tasks (Herting et al. 2011; Weiland et al. 2013; Wetherill et al. 2012). These data suggest that FHA may well affect reward and frontal circuit connectivity, as evident from related work (Cservenka 2016). Broader analyses of whole brain regional network connectivity from resting state studies are less common, but also suggest altered frontal and dorsal premotor and sensorimotor connectivity between those with and without FHA (Holla et al. 2017; Vaidya et al. 2019).

We took a different approach. Rather than trying to distinguish between binary states of rest or cognitive task-related connectivity, we hypothesized that a transitional period between cognitive effort and rest might be more sensitive to FHA. Furthermore, we used a recently proposed, novel data-driven approach (Amico et al. 2017) to decompose whole-brain functional connectomes into independent components driven by inter-subject variability (Fig. S1). This allowed us to isolate functional patterns sensitive to subject characteristics, or other behavioral or genetic variables— in the present case, the FHA-DC (Fig. 2, Fig. S4).

The result was a transient (approximate 3-minute long, Fig. 5) component of connectivity (Fig. 2) that emerged only after the task performance was completed. Those with FHA showed reduced presence of this functional brain reconfiguration, even after accounting for potential nuisance variables (age, sex, task performance, motion) and factors on which the FHA groups differed (depressive symptoms, recent drinking, drinking related problems; Fig. 3). Most importantly, had the analysis tested only for differences within the resting state scans (prior to the task, or in a separate resting state scan some minutes after task completion), or within the task period, this group difference would not have been detected.

Given the anatomic overlap with brain regions involved in the task (Fig. 4), the data also suggest that areas most active during the stop signal task (visual and attentional networks) remain mutually engaged several minutes after the task, with this functional coupling diminishing as subjects resume an introspective rest state (Fig. 5). This brain network reconfiguration process is less harmonized and significantly attenuated in FHA positive subjects (see weights in Fig. 2A3).

Other anatomic features of the FHA-DC included prominent within-network connectivity in the visual system, as well as negative connectivity between the visual network and ventral attention, limbic, frontoparietal, and default mode network areas. Recent studies using group ICA to identify functional connectivity networks find that in comparatively older individuals with more severe alcohol-related problems there is decreased functional connectivity in visual, sensory, and motor areas (Vergara et al. 2017; Vergara et al. 2018). Similarly, machine learning can differentiate alcohol use severity using connectivity features between sensorimotor, default mode, salience, and auditory networks (Fede et al. 2019). Insofar as FHA is a prominent risk for alcoholism, both these current data and findings from other whole brain connectivity studies (Holla et al. 2017; Vaidya et al. 2019) suggest that some of these network features may precede alcohol use.

To our knowledge, this is the first evidence that a brain-based endophenotype of FHA affects FC patterns in the dynamic transition from task engagement to rest. Elsewhere, however, the nature of networks' functional reconfiguration appears to play a prominent role in both cognitive shifts, as well as level of cognitive ability (Schultz and Cole 2016; Shine et al. 2019; Shine et al. 2017; Shine and Poldrack 2018). In this study, we present evidence that such a dynamic reconfiguration in the task-rest transition may be evident in familial risk for alcoholism.

Of particular note, a separate robust "resting-state network-like" (RSN-like) connectivity component (Fig. S4, Fig. S7) emerged across all fMRI blocks that was fundamentally distinct from the FHA-DC component. While this RSN-like component explained an expected large amount of variance (more than 20% of the variance in all blocks), it did *not* differentiate between FHA groups. This pervasive RSN-like component can then be viewed as the "resting-state core", as found in similar, recent studies (Amico et al. 2017; Cole et al. 2014; Contreras et al. 2017), co-occurring in parallel with many other independent connectivity processes (such as, in this case, the FHA-DC). This finding emphasizes the importance of connectivity decomposition to isolate other important processes from the predominant underlying connectivity pattern.

There are some technical considerations in understanding these data. This transitional connectivity reconfiguration was apparent using intermediate and longer sliding window durations (75 – 120 sec, Fig. 5 and Fig. S6). This might be related to two main factors: the functional reconfiguration process could have a characteristic time span (Telesford et al. 2016), and/or the functional connectivity data assessed here could possess noise characteristics that make it difficult to resolve the connectivity pattern at time windows shorter than 75 seconds (Hindriks et al. 2016). We also examined the dynamics using one particular brain parcellation scheme to define the elemental nodes for network analysis. Future studies will need to investigate these factors in more detail, with different task designs, and delve deeper into behavioral (cognitive, emotional) correlates of both the "after-task" reconfiguration, as well as transitional periods from rest to task.

Finally, the question remains as to what this transitional network reconfiguration process might precisely reflect. Two variables were significantly ($p<0.05$) associated with the subjects' individual weights of the FHA-DC: biological sex (Fig. 3A), and delay discounting behavior ($n= 46$ sample, see Fig. S8); a third (depression scores) was significant at a trend level ($p< 0.06$). All three variables relate to alcoholism. Despite a recent narrowing in prevalence, alcoholism remains more common in men (White et al. 2015), who had a significantly smaller FHA-DC (Fig S8). While both family history of alcoholism and delay discounting are potent risk factors and equally heritable (Anokhin et al. 2011; Kaprio et al. 1987; Nurnberger et al. 2004a), FHA positive subjects are not reliably more impulsive than FHA negative subjects (Petry et al. 2002). This suggests the possibility of a low-impulsivity protective factor, similar to high dopamine receptor availability (Volkow et al. 2006) in unaffected FHA positive, which may mediate this variability. FHA is also associated with risks for depression (Nurnberger et al. 2004b), with depression scores in this sample rising with less of the trait, mirroring the FHA pattern. Given the anatomic similarity between the stop signal task activation and the identified FHA-DC, it is also tempting to speculate

that the transient network reorganization process could reflect an “attentional switch” that aids in returning the brain to an introspective-state. Future research will need to parse these potential associations and functions.

Conclusions

A functional connectivity pattern transiently emerged as subjects shifted from an active behavioral state to quiet rest. This functional subsystem is reduced in FHA positive subjects, and primarily involves visual, default-mode, and attentional networks, overlapping anatomically with structures active during the stop signal task. This novel finding suggests that brain endophenotypes of alcoholism (and potentially other kinds of behavioral disorders) may appear in brain network interactions while individuals transition away from external world engagement. The approach holds promise for understanding normal brain function, and more broadly, risk markers for psychiatric illness (Buckholtz and Meyer-Lindenberg 2012).

Supplementary Material

Refer to Web version on PubMed Central for supplementary material.

Acknowledgments

The authors acknowledge important analysis software contributions by Evgeny J. Chumin, insightful comments by Dr. Sarine Janetsian-Fritz, the excellent technical assistance of Dr. Yu-Chien Wu, Dr. Sourajit Mustafi, Michele Dragoo, Traci Day, and Robert Bryant Jr. (MRI facility) as well as study recruitment and implementation by Rachel Baum, Christina Soeurt, Amanda Korsmo, Paige Erb, Tetlu Myint, and Caron Peper. This study is supported by grants from the National Institute on Alcohol Abuse and Alcoholism (Indiana Alcohol Research Center, P60AA07611 to DAK). This work was partially supported by NIH R01EB022574, NIH R01MH108467, and NIH R00AA023296 from the National Institutes of Health. JG acknowledges Purdue Discovery Park Data Science Award (“Fingerprints of the Human Brain: A Data Science Perspective”).

References

Acheson A, Tagamets MA, Rowland LM, Mathias CW, Wright SN, Hong LE, Kochunov P, Dougherty DM. 2014. Increased forebrain activations in youths with family histories of alcohol and other substance use disorders performing a Go/NoGo task. Alcohol Clin Exp Res 38(12):2944–51. [PubMed: 25406902]

Afyouni S, Nichols TE. 2018. Insight and inference for DVARS. Neuroimage 172:291–312. [PubMed: 29307608]

Amico E, Arenas A, Goñi J. 2019. Centralized and distributed cognitive task processing in the human connectome. Network Neuroscience 3(2):455–474. [PubMed: 30793091]

Amico E, Goñi J. 2018. Mapping hybrid functional-structural connectivity traits in the human connectome. Network Neuroscience 2(3):306–322. [PubMed: 30259007]

Amico E, Marinazzo D, Di Perri C, Heine L, Annen J, Martial C, Dzemidzic M, Kirsch M, Bonhomme V, Laureys S et al. . 2017. Mapping the functional connectome traits of levels of consciousness. NeuroImage 148:201–211. [PubMed: 28093358]

Amlung M, Vedelago L, Acker J, Balodis I, MacKillop J. 2017. Steep delay discounting and addictive behavior: a meta-analysis of continuous associations. Addiction 112(1):51–62.

Anokhin AP, Golosheykin S, Grant JD, Heath AC. 2011. Heritability of delay discounting in adolescence: a longitudinal twin study. Behav Genet 41(2):175–83. [PubMed: 20700643]

Anton RF, O’Malley SS, Ciraulo DA, Cisler RA, Couper D, Donovan DM, Gastfriend DR, Hosking JD, Johnson BA, LoCastro JS et al. . 2006. Combined Pharmacotherapies and Behavioral

Interventions for Alcohol Dependence: The COMBINE Study: A Randomized Controlled Trial. JAMA 295(17):2003–2017. [PubMed: 16670409]

Band GPH, van der Molen MW, Logan GD. 2003. Horse-race model simulations of the stop-signal procedure. Acta Psychologica 112(2):105–142. [PubMed: 12521663]

Behrens TEJ, Johansen-Berg H, Woolrich MW, Smith SM, Wheeler-Kingshott CaM, Boulby PA, Barker GJ, Sillery EL, Sheehan K, Ciccarelli O et al. . 2003. Non-invasive mapping of connections between human thalamus and cortex using diffusion imaging. Nature Neuroscience 6(7):750–757. [PubMed: 12808459]

Benjamini Y, Hochberg Y. 1995. Controlling the False Discovery Rate - a Practical and Powerful Approach to Multiple Testing. Journal of the Royal Statistical Society Series B-Statistical Methodology 57(1):289–300.

Bickel WK, Miller ML, Yi R, Kowal BP, Lindquist DM, Pitcock JA. 2007. Behavioral and neuroeconomics of drug addiction: competing neural systems and temporal discounting processes. Drug Alcohol Depend 90 Suppl 1:S85–91. [PubMed: 17101239]

Braun U, Schafer A, Walter H, Erk S, Romanczuk-Seiferth N, Haddad L, Schweiger JI, Grimm O, Heinz A, Tost H et al. . 2015. Dynamic reconfiguration of frontal brain networks during executive cognition in humans. Proc Natl Acad Sci U S A 112(37):11678–83. [PubMed: 26324898]

Bucholz KK, Cadoret R, Cloninger CR, Dinwiddie SH, Hesselbrock VM, Nurnberger JI, Reich T, Schmidt I, Schuckit MA. 1994. A new, semi-structured psychiatric interview for use in genetic linkage studies: a report on the reliability of the SSAGA. Journal of Studies on Alcohol 55(2):149–158. [PubMed: 8189735]

Buckholtz JW, Meyer-Lindenberg A. 2012. Psychopathology and the human connectome: toward a transdiagnostic model of risk for mental illness. Neuron 74(6):990–1004. [PubMed: 22726830]

Calhoun VD, Adali T, Giuliani NR, Pekar JJ, Kiehl KA, Pearlson GD. 2006. Method for multimodal analysis of independent source differences in schizophrenia: combining gray matter structural and auditory oddball functional data. Human Brain Mapping 27(1):47–62. [PubMed: 16108017]

Calhoun VD, Liu J, Adalı T. 2009. A review of group ICA for fMRI data and ICA for joint inference of imaging, genetic, and ERP data. NeuroImage 45(1):S163–S172. [PubMed: 19059344]

Chen RH, Ito T, Kulkarni KR, Cole MW. 2018. The Human Brain Traverses a Common Activation-Pattern State Space Across Task and Rest. Brain Connectivity 8(7):429–443. [PubMed: 29999413]

Cohen E, Feinn R, Arias A, Kranzler HR. 2007. Alcohol treatment utilization: Findings from the National Epidemiologic Survey on Alcohol and Related Conditions. Drug and Alcohol Dependence 86(2):214–221. [PubMed: 16919401]

Cole Michael W, Bassett Danielle S, Power Jonathan D, Braver Todd S, Petersen Steven E. 2014. Intrinsic and Task-Evoked Network Architectures of the Human Brain. Neuron 83(1):238–251. [PubMed: 24991964]

Colrain IM. 2015. Family history of alcoholism and brain activation: commentary on “Increased forebrain activations in youths with family histories of alcohol and other substance use disorders performing a Go/No-Go task”. Alcohol Clin Exp Res 39(3):403–4. [PubMed: 25704052]

Contreras JA, Goñi J, Risacher SL, Amico E, Yoder K, Dzemidzic M, West JD, McDonald BC, Farlow MR, Sporns O et al. . 2017. Cognitive complaints in older adults at risk for Alzheimer’s disease are associated with altered resting-state networks. Alzheimer’s and Dementia: Diagnosis, Assessment and Disease Monitoring 6:40–49.

Cservenka A. 2016. Neurobiological phenotypes associated with a family history of alcoholism. Drug Alcohol Depend 158:8–21. [PubMed: 26559000]

Cservenka A, Casimo K, Fair DA, Nagel BJ. 2014. Resting state functional connectivity of the nucleus accumbens in youth with a family history of alcoholism. Psychiatry Research: Neuroimaging 221(3):210–219. [PubMed: 24440571]

Dougherty DM, Lake SL, Mathias CW, Ryan SR, Bray BC, Charles NE, Acheson A. 2015. Behavioral Impulsivity and Risk-Taking Trajectories Across Early Adolescence in Youths With and Without Family Histories of Alcohol and Other Drug Use Disorders. Alcoholism: Clinical and Experimental Research 39(8):1501–1509.

Du W, Green L, Myerson J. 2002. Cross-cultural comparisons of discounting delayed and probabilistic rewards. The Psychological Record 52(4):479–92.

Fede SJ, Grodin EN, Dean SF, Diazgranados N, Momenan R. 2019. Resting state connectivity best predicts alcohol use severity in moderate to heavy alcohol users. Neuroimage Clin 22:101782. [PubMed: 30921611]

Fernie G, Peeters M, Gullo MJ, Christiansen P, Cole JC, Sumnall H, Field M. 2013. Multiple behavioural impulsivity tasks predict prospective alcohol involvement in adolescents. Addiction 108(11):1916–23. [PubMed: 23795646]

Gallen CL, Turner GR, Adnan A, D'Esposito M. 2016. Reconfiguration of brain network architecture to support executive control in aging. Neurobiol Aging 44:42–52. [PubMed: 27318132]

Gonzalez-Castillo J, Bandettini PA. 2018. Task-based dynamic functional connectivity: Recent findings and open questions. NeuroImage 180:526–533. [PubMed: 28780401]

Grant BF, Goldstein RB, Saha TD, Chou SP, Jung J, Zhang H, Pickering RP, Ruan WJ, Smith SM, Huang B et al. . 2015. Epidemiology of DSM-5 Alcohol Use Disorder: Results From the National Epidemiologic Survey on Alcohol and Related Conditions III. JAMA Psychiatry 72(8):757–766. [PubMed: 26039070]

Greve DN, Fischl B. 2009. Accurate and robust brain image alignment using boundary-based registration. NeuroImage 48(1):63–72. [PubMed: 19573611]

Gustavson DE, Stallings MC, Corley RP, Miyake A, Hewitt JK, Friedman NP. 2017. Executive functions and substance use: Relations in late adolescence and early adulthood. Journal of Abnormal Psychology 126(2):257–270. [PubMed: 28045282]

Hardee JE, Weiland BJ, Nichols TE, Welsh RC, Soules ME, Steinberg DB, Zubieta J-K, Zucker RA, Heitzeg MM. 2014. Development of Impulse Control Circuitry in Children of Alcoholics. Biological Psychiatry 76(9):708–716. [PubMed: 24742620]

Heiman GA, Ogburn E, Gorroochurn P, Keyes KM, Hasin D. 2008. Evidence for a two-stage model of dependence using the NESARC and its implications for genetic association studies. Drug and Alcohol Dependence 92(1):258–266. [PubMed: 17933473]

Herting MM, Fair D, Nagel BJ. 2011. Altered fronto-cerebellar connectivity in alcohol-naïve youth with a family history of alcoholism. NeuroImage 54(4):2582–2589. [PubMed: 20970506]

Hindriks R, Adhikari MH, Murayama Y, Ganzetti M, Mantini D, Logothetis NK, Deco G. 2016. Can sliding-window correlations reveal dynamic functional connectivity in resting-state fMRI? NeuroImage 127:242–256. [PubMed: 26631813]

Holla B, Panda R, Venkatasubramanian G, Biswal B, Bharath RD, Benegal V. 2017. Disrupted resting brain graph measures in individuals at high risk for alcoholism. Psychiatry Research: Neuroimaging 265:54–64. [PubMed: 28531764]

Hyvarinen A. 1999. Fast and robust fixed-point algorithms for independent component analysis. IEEE Transactions on Neural Networks 10(3):626–634. [PubMed: 18252563]

Hyvärinen A, Oja E. 2000. Independent component analysis: algorithms and applications. Neural Networks 13(4):411–430. [PubMed: 10946390]

Jenkinson M, Beckmann CF, Behrens TEJ, Woolrich MW, Smith SM. 2012. FSL. NeuroImage 62(2):782–790. [PubMed: 21979382]

Johnson MW, Bickel WK. 2008. An algorithm for identifying nonsystematic delay-discounting data. Exp Clin Psychopharmacol 16(3):264–74. [PubMed: 18540786]

Jolliffe I. 2014. Principal Component Analysis. Wiley StatsRef: Statistics Reference Online. John Wiley & Sons, Ltd.

Kaprio J, Koskenvuo M, Langinvainio H, Romanov K, Sarna S, Rose RJ. 1987. Genetic influences on use and abuse of alcohol: a study of 5638 adult Finnish twin brothers. Alcoholism: Clinical and Experimental Research 11(4):349–356.

Kareken DA, Dzemidzic M, Wetherill L, Eiler W, Oberlin BG, Harezlak J, Wang Y, O'Connor SJ. 2013. Family history of alcoholism interacts with alcohol to affect brain regions involved in behavioral inhibition. Psychopharmacology 228(2):335–345. [PubMed: 23468100]

Kessler D, Angstadt M, Welsh RC, Sripada C. 2014. Modality-Spanning Deficits in Attention-Deficit/Hyperactivity Disorder in Functional Networks, Gray Matter, and White Matter. Journal of Neuroscience 34(50):16555–16566. [PubMed: 25505309]

Lewis CM, Baldassarre A, Committeri G, Romani GL, Corbetta M. 2009. Learning sculpts the spontaneous activity of the resting human brain. Proceedings of the National Academy of Sciences 106(41):17558–17563.

Logan GD, Cowan WB. 1984. On the ability to inhibit thought and action: A theory of an act of control. Psychological Review 91(3):295–327.

MacKillop J, Kahler CW. 2009. Delayed reward discounting predicts treatment response for heavy drinkers receiving smoking cessation treatment. Drug Alcohol Depend 104(3):197–203. [PubMed: 19570621]

Mawlawi O, Martinez D, Slifstein M, Broft A, Chatterjee R, Hwang D-R, Huang Y, Simpson N, Ngo K, Van Heertum R et al. . 2001. Imaging Human Mesolimbic Dopamine Transmission with Positron Emission Tomography: I. Accuracy and Precision of D2 Receptor Parameter Measurements in Ventral Striatum. Journal of Cerebral Blood Flow & Metabolism 21(9):1034–1057. [PubMed: 11524609]

Mennes M, Kelly C, Zuo XN, Di Martino A, Biswal BB, Castellanos FX, Milham MP. 2010. Inter-individual differences in resting-state functional connectivity predict task-induced BOLD activity. Neuroimage 50(4):1690–701. [PubMed: 20079856]

Moss HB, Chen CM, Yi H-y. 2007. Subtypes of alcohol dependence in a nationally representative sample. Drug and Alcohol Dependence 91(2):149–158. [PubMed: 17597309]

Nigg JT, Glass JM, Wong MM, Poon E, Jester JM, Fitzgerald HE, Puttler LI, Adams KM, Zucker RA. 2004. Neuropsychological Executive Functioning in Children at Elevated Risk for Alcoholism: Findings in Early Adolescence. Journal of Abnormal Psychology 113(2):302–314. [PubMed: 15122950]

Nurnberger JI Jr., Wiegand R, Bucholz K, O'Connor S, Meyer ET, Reich T, Rice J, Schuckit M, King L, Petti T et al. . 2004a. A family study of alcohol dependence: coaggregation of multiple disorders in relatives of alcohol-dependent probands. Arch Gen Psychiatry 61(12):1246–56. [PubMed: 15583116]

Nurnberger JI, Wiegand R, Bucholz K, O'Connor S, Meyer ET, Reich T, Rice J, Schuckit M, King L, Petti T et al. . 2004b. A Family Study of Alcohol Dependence: Coaggregation of Multiple Disorders in Relatives of Alcohol-DependentProbands. Archives of General Psychiatry 61(12):1246–1256. [PubMed: 15583116]

Petry NM, Kirby KN, Kranzler HR. 2002. Effects of gender and family history of alcohol dependence on a behavioral task of impulsivity in healthy subjects. J Stud Alcohol 63(1):83–90. [PubMed: 11925063]

Porjesz B, Rangaswamy M, Kamarajan C, Jones KA, Padmanabhapillai A, Begleiter H. 2005. The utility of neurophysiological markers in the study of alcoholism. Clinical Neurophysiology 116(5):993–1018. [PubMed: 15826840]

Power JD, Barnes KA, Snyder AZ, Schlaggar BL, Petersen SE. 2012. Spurious but systematic correlations in functional connectivity MRI networks arise from subject motion. NeuroImage 59(3):2142–2154. [PubMed: 22019881]

Power JD, Mitra A, Laumann TO, Snyder AZ, Schlaggar BL, Petersen SE. 2014. Methods to detect, characterize, and remove motion artifact in resting state fMRI. NeuroImage 84:320–341. [PubMed: 23994314]

Pyka M, Beckmann CF, Schöning S, Hauke S, Heider D, Kugel H, Arolt V, Konrad C. 2009. Impact of Working Memory Load on fMRI Resting State Pattern in Subsequent Resting Phases. PLOS ONE 4(9):e7198. [PubMed: 19779619]

Raichle ME, MacLeod AM, Snyder AZ, Powers WJ, Gusnard DA, Shulman GL. 2001. A default mode of brain function. Proceedings of the National Academy of Sciences 98(2):676–682.

Särelä J, Vigário R. 2003. Overlearning in Marginal Distribution-Based ICA: Analysis and Solutions. Journal of Machine Learning Research 4(Dec):1447–1469.

Schneekloth TD, Biernacka JM, Hall-Flavin DK, Karpyak VM, Frye MA, Loukianova LL, Stevens SR, Drews MS, Geske JR, Mrazek DA. 2012. Alcohol Craving as a Predictor of Relapse. The American Journal on Addictions 21(s1):S20–S26. [PubMed: 23786506]

Schultz DH, Cole MW. 2016. Higher Intelligence Is Associated with Less Task-Related Brain Network Reconfiguration. Journal of Neuroscience 36(33):8551–8561. [PubMed: 27535904]

Shen X, Tokoglu F, Papademetris X, Constable RT. 2013. Groupwise whole-brain parcellation from resting-state fMRI data for network node identification. NeuroImage 82:403–415. [PubMed: 23747961]

Shine JM, Breakspear M, Bell PT, Martens KAE, Shine R, Koyejo O, Sporns O, Poldrack RA. 2019. Human cognition involves the dynamic integration of neural activity and neuromodulatory systems. Nature Neuroscience 22(2):289. [PubMed: 30664771]

Shine JM, Kucyi A, Foster BL, Bickel S, Wang D, Liu H, Poldrack RA, Hsieh L-T, Hsiang JC, Parvizi J. 2017. Distinct Patterns of Temporal and Directional Connectivity among Intrinsic Networks in the Human Brain. Journal of Neuroscience 37(40):9667–9674. [PubMed: 28893929]

Shine JM, Poldrack RA. 2018. Principles of dynamic network reconfiguration across diverse brain states. NeuroImage 180:396–405. [PubMed: 28782684]

Shulman GL, Corbetta M, Buckner RL, Fiez JA, Miezin FM, Raichle ME, Petersen SE. 1997. Common Blood Flow Changes across Visual Tasks: I. Increases in Subcortical Structures and Cerebellum but Not in Nonvisual Cortex. Journal of Cognitive Neuroscience 9(5):624–647. [PubMed: 23965121]

Smith SM, Jenkinson M, Woolrich MW, Beckmann CF, Behrens TEJ, Johansen-Berg H, Bannister PR, De Luca M, Drobnjak I, Flitney DE et al. . 2004. Advances in functional and structural MR image analysis and implementation as FSL. NeuroImage 23:S208–S219. [PubMed: 15501092]

Stanger C, Ryan SR, Fu H, Landes RD, Jones BA, Bickel WK, Budney AJ. 2012. Delay discounting predicts adolescent substance abuse treatment outcome. Exp Clin Psychopharmacol 20(3):205–12. [PubMed: 22182419]

Telesford QK, Lynall M-E, Vettel J, Miller MB, Grafton ST, Bassett DS. 2016. Detection of functional brain network reconfiguration during task-driven cognitive states. NeuroImage 142:198–210. [PubMed: 27261162]

Vaidya JG, Elmore AL, Wallace A, Langbehn DR, Kramer JR, Kuperman S, O'Leary DS. 2019. Association Between Age and Familial Risk for Alcoholism on Functional Connectivity in Adolescence. Journal of the American Academy of Child & Adolescent Psychiatry.

Vergara VM, Liu J, Claus ED, Hutchison K, Calhoun V. 2017. Alterations of resting state functional network connectivity in the brain of nicotine and alcohol users. Neuroimage 151:45–54. [PubMed: 27864080]

Vergara VM, Weiland BJ, Hutchison KE, Calhoun VD. 2018. The Impact of Combinations of Alcohol, Nicotine, and Cannabis on Dynamic Brain Connectivity. Neuropsychopharmacology 43(4):877–890. [PubMed: 29134961]

Volkow ND, Wang GJ, Begleiter H, Porjesz B, Fowler JS, Telang F, Wong C, Ma Y, Logan J, Goldstein R et al. . 2006. High levels of dopamine D2 receptors in unaffected members of alcoholic families: possible protective factors. Arch Gen Psychiatry 63(9):999–1008. [PubMed: 16953002]

Walters RK, Polimanti R, Johnson EC, McClintick JN, Adams MJ, Adkins AE, Aliev F, Bacanu S-A, Batzler A, Bertelsen S et al. . 2018. Transancestral GWAS of alcohol dependence reveals common genetic underpinnings with psychiatric disorders. Nature Neuroscience 21(12):1656. [PubMed: 30482948]

Weiland BJ, Welsh RC, Yau W-YW, Zucker RA, Zubieta J-K, Heitzeg MM. 2013. Accumbens functional connectivity during reward mediates sensation-seeking and alcohol use in high-risk youth. Drug and Alcohol Dependence 128(1):130–139. [PubMed: 22958950]

Wetherill RR, Bava S, Thompson WK, Boucquey V, Pulido C, Yang TT, Tapert SF. 2012. Frontoparietal connectivity in substance-naïve youth with and without a family history of alcoholism. Brain Research 1432:66–73. [PubMed: 22138427]

Whelan R, Watts R, Orr CA, Althoff RR, Artiges E, Banaschewski T, Barker GJ, Bokde ALW, Büchel C, Carvalho FM et al. . 2014. Neuropsychosocial profiles of current and future adolescent alcohol misusers. Nature 512(7513):185–189. [PubMed: 25043041]

White A, Castle IJP, Chen CM, Shirley M, Roach D, Hingson R. 2015. Converging Patterns of Alcohol Use and Related Outcomes Among Females and Males in the United States, 2002 to 2012. Alcoholism: Clinical and Experimental Research 39(9):1712–1726.

Xu J, Moeller S, Auerbach EJ, Strupp J, Smith SM, Feinberg DA, Yacoub E, Uğurbil K. 2013. Evaluation of slice accelerations using multiband echo planar imaging at 3T. NeuroImage 83:991–1001. [PubMed: 23899722]

Yeo TBT, Krienen FM, Sepulcre J, Sabuncu MR, Lashkari D, Hollinshead M, Roffman JL, Smoller JW, Zöllei L, Polimeni JR et al. . 2011. The organization of the human cerebral cortex estimated by intrinsic functional connectivity. Journal of Neurophysiology 106(3):1125–1165. [PubMed: 21653723]

Young SE, Friedman NP, Miyake A, Willcutt EG, Corley RP, Haberstick BC, Hewitt JK. 2009. Behavioral disinhibition: liability for externalizing spectrum disorders and its genetic and environmental relation to response inhibition across adolescence. Journal of abnormal psychology 118(1):117–130. [PubMed: 19222319]

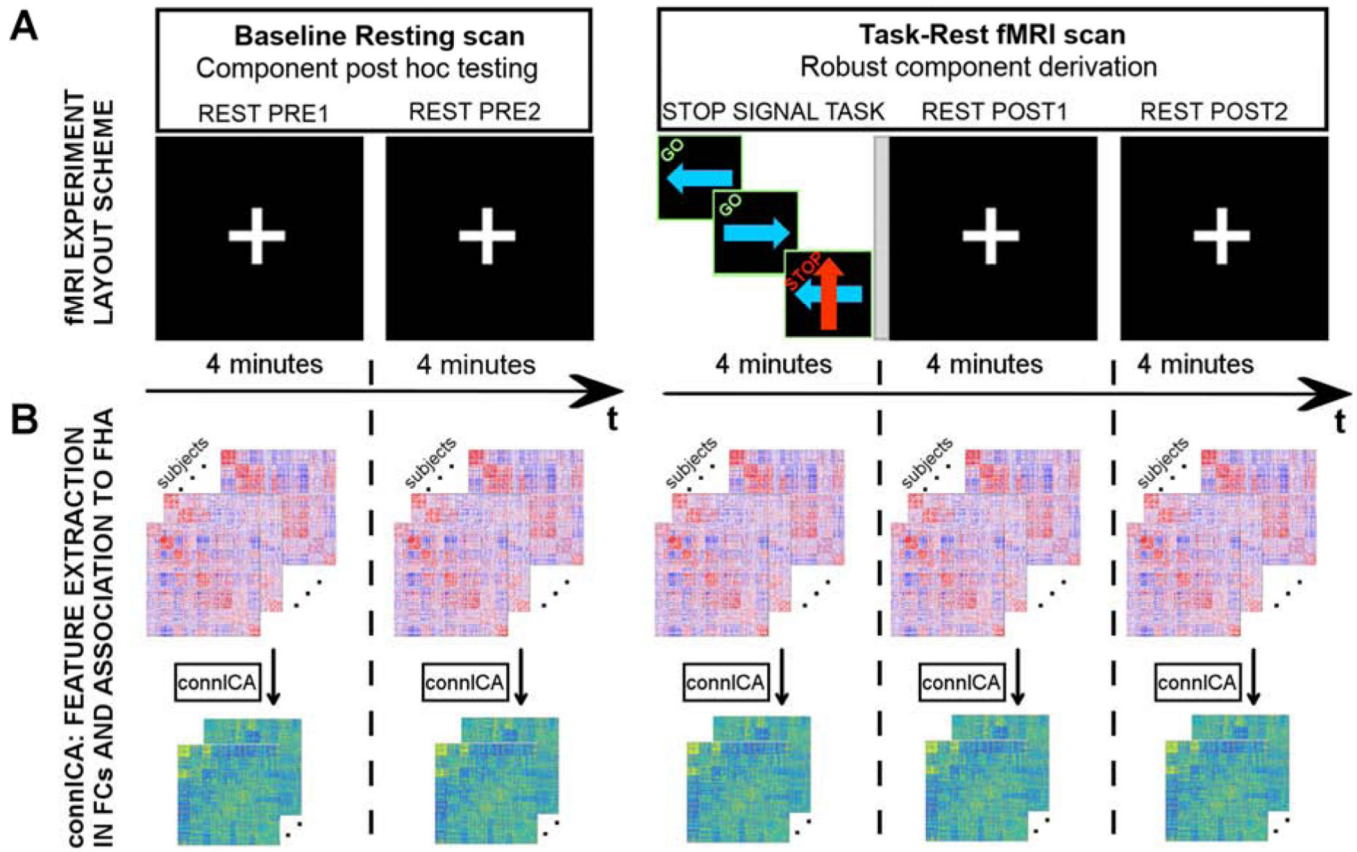

Fig. 1. Study design and functional connectivity (FC) analysis scheme.

A) Each subject completed two fMRI scans: a baseline resting scan (*left*), with eyes fixated on a central white cross-hair; a task-rest fMRI scan (*right*) comprised a 4 minute stop signal task (Logan and Cowan 1984) in which the direction of a blue arrow prompted a left or right button press and a red arrow indicated the need to withhold the response to a blue arrow (labels on top of each tile are only illustrative and did not appear on the actual stimuli). Within this same scan the task was followed by a short 12 sec intermission (indicated by a gray vertical stripe rectangle) when a slide announced the upcoming rest with the printed statement, "The task is over. Fix your gaze on the cross-hair for the remainder of the scan". Subjects then rested for 8 minutes and again fixated on a white central cross-hair. **B)** Both fMRI scans were subdivided into 4 minute "static" segments (blocks), for which we independently estimated whole-brain functional connectomes and obtained independent connectivity components using the connICA method.

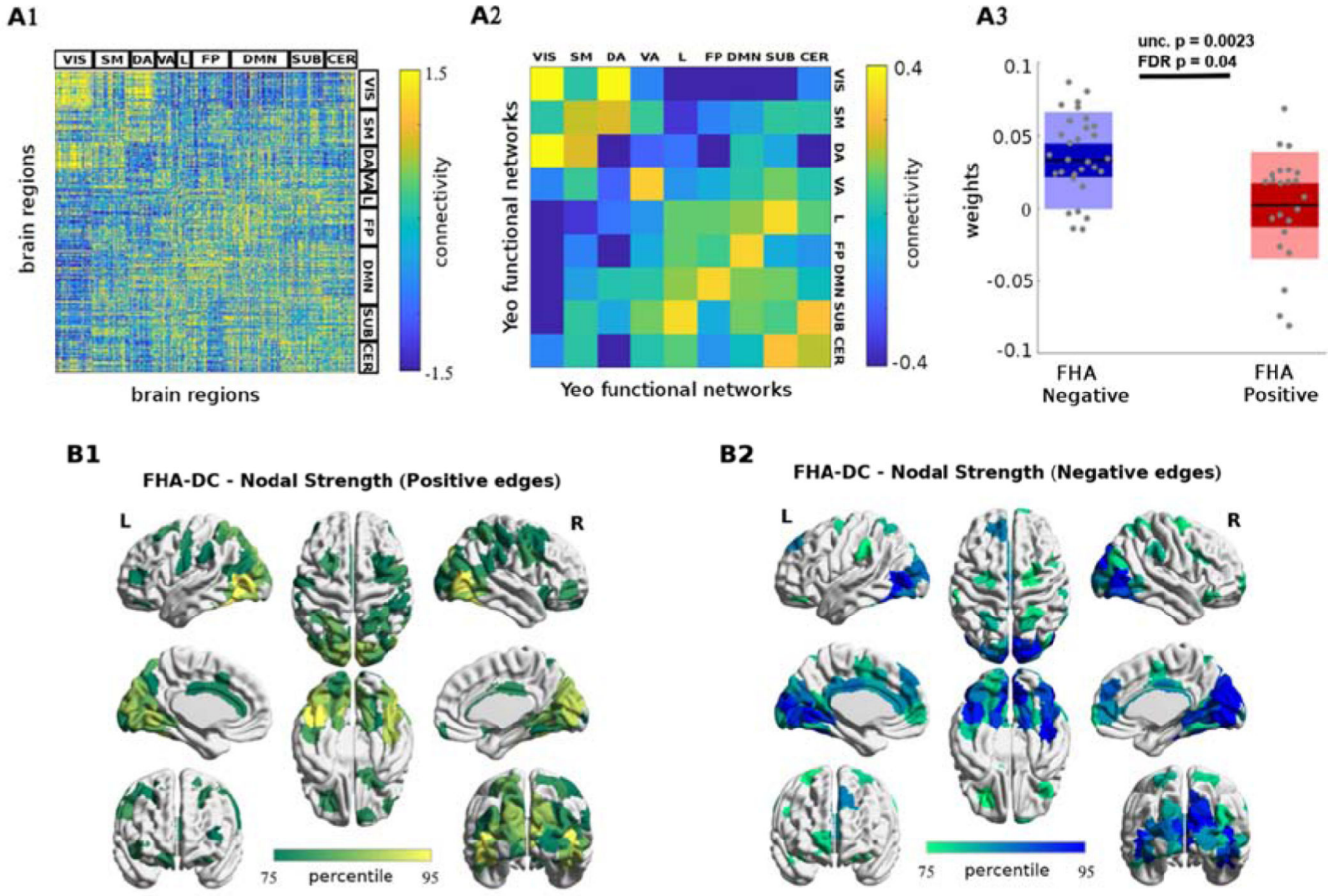

Fig. 2. Family history of alcoholism differentiating component (FHA-DC).

A1) The functional connectivity reconfiguration component extracted by connICA in the REST POST1 window (i.e., within 4 minutes after completing the stop signal task). Pairwise associations between brain regions are ordered by resting-state functional networks as proposed by Yeo et al. (Yeo et al. 2011). **A2)** For clarity, the same component, depicted after averaging across functional networks, shows prominent connectivity between the visual and dorsal attention network areas, as well as between default-mode and frontoparietal networks. **A3)** Group differences in the individual subject weights associated with FHA-DC (two-tailed *t*-test between FHA negative and positive groups, p=0.0023; False Discovery Rate (FDR, (Benjamini and Hochberg 1995) adjusted p=0.04, accounting for the 30 robust components); see A3 and B). **B1-B2)** Nodal strength (sum over columns of **A1,** including only: **B1)** positive edges or **B2)** negative edges) of the top 25% regions involved in the identified FHA-differentiating component.

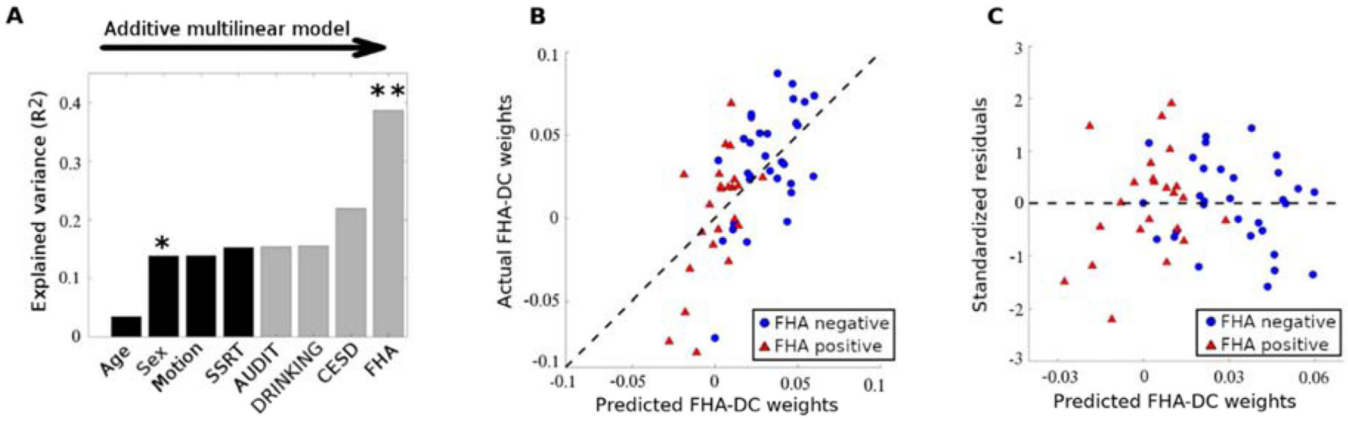

Fig. 3. FHA-DC individual weights predictability by family history of alcoholism, after accounting for possible confounds.

A) Additive multi-linear regression model with predictors sequentially introduced in the order of: age, sex, head motion (number of scrubbed volumes), stop-signal response time (SSRT), AUDIT score, normalized drinking (see Methods), depression score (CESD), and FHA group membership. Significant predictors are indicated by one or two asterisks ($p<0.05$ and $p<0.01$, respectively). **B)** Scatter plot of the subject weights (average across connICA runs) associated with the extracted FHA-differentiating component versus the subject weights predicted by the final multi-linear regression model that includes all eight predictors in (A). Blue circles represent individual weights for the FHA negative group, red triangles represent individual weights for the FHA positive group. Dashed black line represents the identity line. **C)** Scatter plot of the standardized residuals versus the predicted subject weights associated with the FHA-DC for the multi-linear model shown in (A) (also see Methods for details).

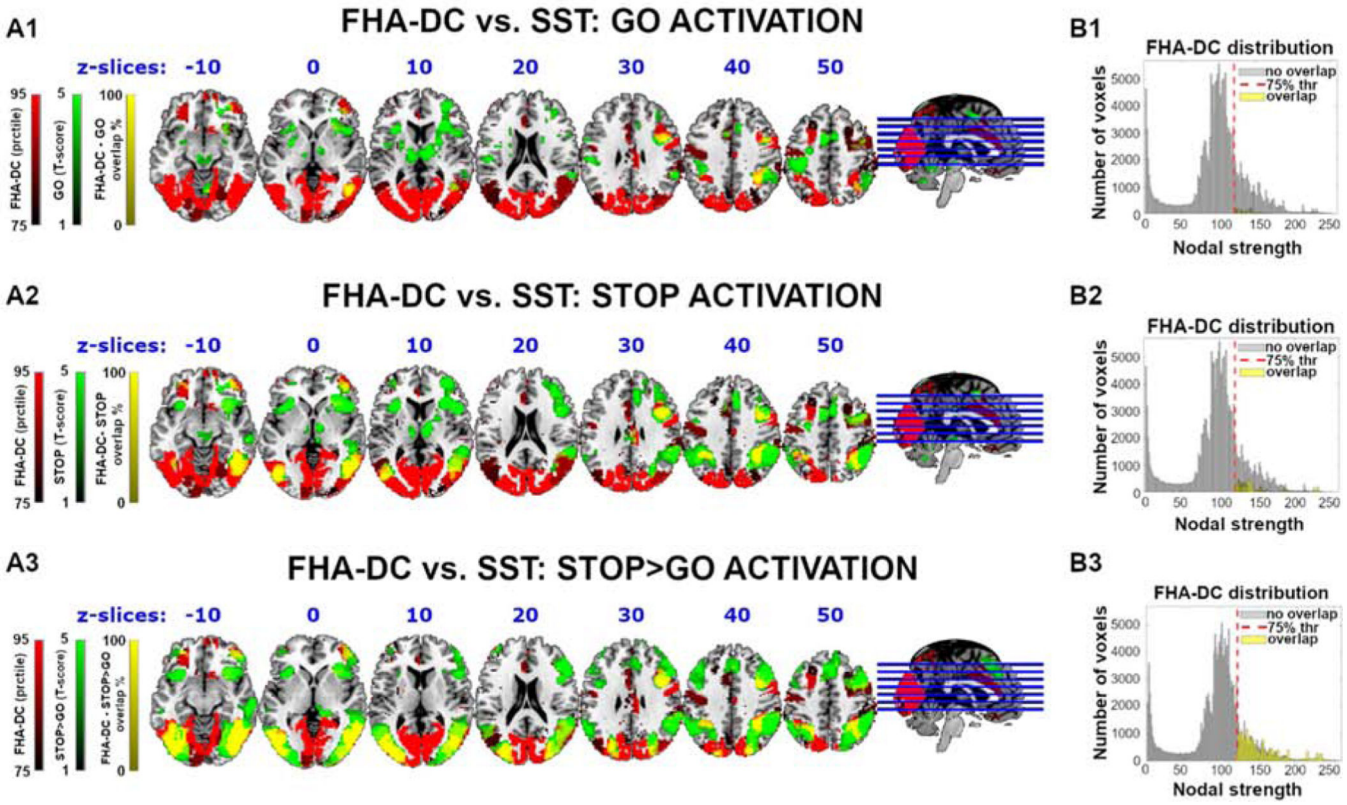

Fig. 4. Spatial overlap of brain regions engaged during stop signal task and top 25% nodal strength positive edges in the FHA-DC during REST-POST1 block.

SST responding regions to **(A1)** successful GO trials, **(A2)** successfully inhibited Stop trials, **(A3)** the successful Stop > Go trials BOLD contrast (green overlay, *t*-statistic, voxel-wise FWE cluster-corrected at $p<0.05$, $p=0.001$ cluster-defining threshold). Red represents the most prominent regions (top 25% in nodal strength, including positive edges only) of the FHA-DC. The spatial overlap between BOLD activation and the anatomic distribution of the FHA-DC is most prominent in frontoparietal and lateral occipito-temporal regions (yellow overlay). **(B1-B3)** Histogram of the distribution of FHA-DC voxels that do (yellow bars), and do not (gray bars) overlap with the SST activation maps in (A1-A3). The [Stop>Go] contrast, which depicts highly engaged brain regions, overlaps the most and occurs along the right tails of the histogram, where the nodal strength of the FHA-differentiating component is greatest (red dashed lines indicate 75% nodal strength threshold; Thr). Axial slices ("z-slices" in the figure, in mm) indicate Montreal Neurological Institute (MNI) coordinate values.

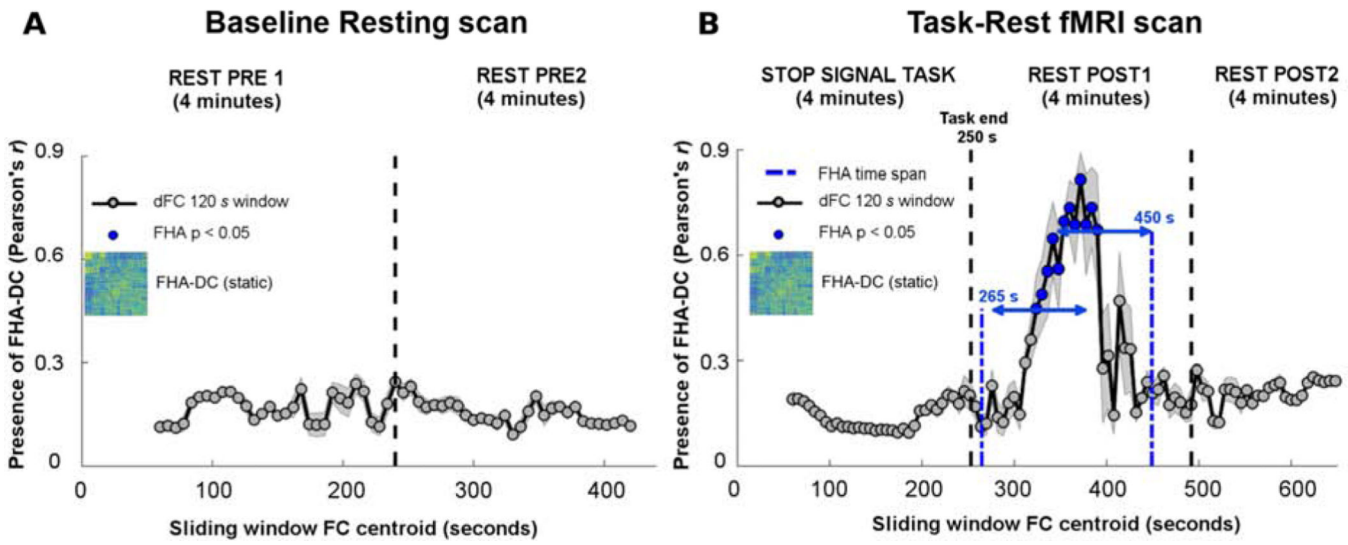

Fig. 5. Dynamics of the FHA-DC during both fMRI scans.

4A-4B). We ran connICA on each 120 second sliding window during the baseline resting scan **(A)** and task-rest fMRI scan **(B)**. The presence of the component (as reflected by Pearson's correlation coefficient, r) includes all subjects, regardless of the FHA status. The best matching correlation between the dynamic FC-component and the "static" FHA-DC (left inset, from Fig. 2A3) is shown across each sliding window centroid. Matching between components was measured by Pearson's correlation coefficient between the (vectorized) connectivity profiles. Vertical dashed lines indicate the separation between 4-minute "static" blocks (Figs. 1 and 2). Shaded gray bars indicate standard deviation across 25 bootstrap runs (see Methods for details). Blue dots indicate dynamic functional connectivity windows during which FHA groups significantly differ ($p < 0.05$), starting approximately 20 seconds after task cessation, and lasting for about 3 min, with an average peak correlation with the FHA-DC static result of 0.85 ± 0.15. Note the absence of significant correlations (on average 0.15 ± 0.05) between the originally extracted FHA-DC during REST POST1 and connectivity during the baseline resting scan as assessed using the sliding window.

Table 1.

Subject Characteristics (N = 54)

	FHA positive (n=23, 9 men)		FHA negative (n=31, 16 men)	
	Mean (SD)	**Range**	**Mean (SD)**	**Range**
Age	23.04 (± 1.64)	21–26	22.35 (± 1.58)	21–26
Education (years)	15.32 (± 1.25)	13–18	15.23 (± 1.20)	14–19
SSRT[a] (ms)	250 (± 48)	157–397	230 (± 52)	124–346
AUDIT[b]	10.26 (± 6.52) *	2–29	7.26 (± 3.92)	1–20
CESD[c]	8.04 (± 5.52) *	1–24	4.57 (± 4.21)	0–17
Drinks per week	12.27(± 11.46) *	1.80–51.40	7.12 (± 4.91)	1.20–20.80
Alcohol Grams/Week TBW[d] normalized	3.59 (± 2.77) *	0.79–11.77	2.25 (± 1.66)	0.25–7.98

[a] Stop Signal Response Time; time to withdraw a response

[b] Alcohol Use Disorders Identification Test

[c] Center for Epidemiologic Studies Depression scale

[d] Total Body Water

* FHA significant difference, two-tailed *t*-test $p < 0.05$